Available online at www.sciencedirect.com
ScienceDirect
Journal of Power Sources 171 (2007) 999–1009
JOURNAL OF POWER SOURCES
www.elsevier.com/locate/jpowsour

A new powder morphology for making high-porosity nickel structures

Elena Cormier [a], Eric Bain Wasmund [b,*], Les V. Renny [b], Quan Min Yang [a], Doug Charles [a]

[a] *Inco Technical Services Limited, Mississauga, Ont., Canada L5K 1Z9*
[b] *Inco Special Products, Mississauga, Ont., Canada L5K 2L3*

Received 3 May 2007; received in revised form 18 June 2007; accepted 20 June 2007
Available online 3 July 2007

Abstract

Nickel powders with a special branched chain microstructure such as CVRD Inco Limited's Type 255™ have been used for more than 50 years as the basis for making porous metal monoliths for applications such as the electrical backbone of nickel electrode batteries by the sinter/slurry process. The classic trade-off when making these structures is that the strength and porosity are inversely correlated. A number of adaptations to the sinter/slurry making process have been proposed to address this problem. The current approach proposes another solution, optimization of the particle microstructure. The strength and porosity relationship of battery plaques made from Type 255™ is compared with plaques made with the new powder and it is statistically verified that plaques made from the new powder have an improved combination of structural properties. A comparison of the rheological characteristics of metal powder slurries suggests ways that the new powder can be incorporated into existing processes. Finally, it is shown that properties such as the slurry apparent viscosity can be used as the basis for measuring and predicting the characteristics of particle microstructure that impute these benefits to the sinter/slurry process. An analysis of battery plaques made with the new powder on an industrial battery sinter/slurry production line confirms that the laboratory results are valid.

Keywords: Nickel batteries; Sintered electrodes; Rheology; Porosity

1. Introduction

Rechargeable batteries using nickel electrodes are used in a wide variety of industry and consumer segments such as cordless power tools, hybrid electric vehicles, aviation and rail and consumer applications. In these applications, the positive electrode consists of nickel hydroxide, which is the active material, intimately bonded to a nickel current collector. The half-cell reaction for nickel hydroxide is shown in Eq. (1). The vast majority of the electrodes for these applications are pasted nickel foam or sintered nickel powder. The former type is made by pasting a slurry of nickel hydroxide into nickel foam, an open cell nickel-based structure, followed by drying and calendering to the final electrode thickness. The latter type is made by sintering nickel powder to a nickel-plated steel substrate to make a nickel plaque structure, and then chemically or electrochemically impregnating the plaque with nickel hydroxide by successive dipping of nickel salts and caustic [1]. To achieve a highly porous structure, the nickel powder used for making sintered electrodes must consist of three-dimensional chains, such as CVRD Inco's Type 255™ nickel powder. In the case of high-quality nickel cadmium cells, Type 255™ powder is also used as a binder for the cadmium electrode:

$$\mathrm{NiOOH} + \mathrm{HOH} + \mathrm{e}^- \rightarrow \mathrm{Ni(OH)_2} + \mathrm{OH}^- \quad (1)$$

One of the advantages of the pasted foam process is that the nickel foam has a much lower contribution to the volume of the electrode than the nickel powder in a sintered electrode. This means that the ratio of nickel current collector to active material is reduced, which increases the energy density and lowers the cost of the battery raw materials. On the other hand, in a sintered electrode, the pores containing nickel hydroxide are on average, an order of magnitude smaller than a foam pore. This decreases on average the distance for electrons to travel from the current collector into the active material during cell discharge, and consequently improves the discharge rate characteristics. This is one of the reasons that sintered nickel electrodes still dominate the cordless power tool application. Therefore, each type of electrode has advantages and disadvantages, the pasted foam design

* Corresponding author. Tel.: +1 905 403 3371; fax: +1 905 403 8132.
E-mail address: ewasmund@inco.com (E.B. Wasmund).

0378-7753/$ – see front matter © 2007 Elsevier B.V. All rights reserved.
doi:10.1016/j.jpowsour.2007.06.253

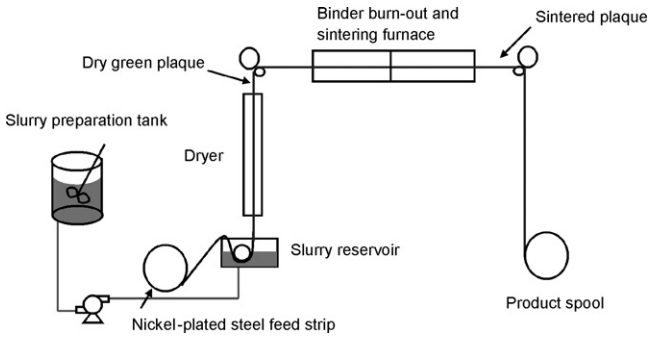

Fig. 1. A generic schematic of a continuous sinter/slurry line for making porous nickel plaques for rechargeable batteries.

uses less inactive nickel in the electrode, and the sintered powder design has better discharge characteristics and cell longevity. This work focuses on the development of new nickel powders that open the door to making sintered nickel powder electrodes with equivalent performance and a reduction in the amount of nickel required in the plaque of approximately 20%.

To understand the challenge of making improved nickel powder for manufacturing sintered plaques, it is necessary to provide a simplified overview of the sinter/slurry process. A generic schematic is shown in Fig. 1. In the first step, the nickel powder is dispersed in an aqueous solution of an organic binder such as methyl cellulose in a slurry preparation tank. The nickel powder paste is then pumped to the slurry reservoir in a pasting line. In the second step, a perforated metal strip is drawn through the slurry reservoir and becomes coated on both sides with the nickel paste. The excess paste on both sides is removed with a pair of doctor blades, similar to those used in standard tape-casting processes. The apparent viscosity of the paste as it goes past the doctor blades will influence the thickness of the paste coating. The distance of separation between the blades also influences the coating thickness. In the third step, the paste coating is dried. In the green state, the nickel powder is held to the metal strip with the binder, this product will be referred to as the green plaque. In the fourth step, the nickel powder strip is fired in a two-stage furnace. In the first furnace stage, the binder is removed in an oxidizing atmosphere. In the second furnace stage, the nickel powder is sintered under a slightly reducing atmosphere to form a solid porous structure that is bonded to the metal strip. This will be referred to as the sintered plaque.

The sintering step is very important because it essentially controls two key characteristics of the plaque, the porosity and the plaque strength. In general, both of these properties are important in the sintered electrode; higher porosity allows the inclusion of more active material in the electrode, and strength is important to resist volume changes during cycling and to provide adhesion to the metal strip as the electrode is wound for making cylindrical cells.

Modifications to the conditions of the plaque-making process shown in Fig. 1 can be made to adjust the porosity and strength, however under normal conditions, the resulting porosity and strength are inversely correlated, so that an increase in one of these parameters is at the expense of a negative gain in the other. In previous works, innovations have been proposed to increase the strength by improving the nickel slurry dispersion [2] or by pre-coating the metal strip with extrafine nickel powder [3]. In this paper, we will show how a new nickel powder with an optimized particle structure can allow an improvement in both parameters, which has the effect of increasing the porosity at the same level of strength.

2. Experimental/materials and methods

Inco Limited, and now CVRD Inco Limited has for many years produced a family of unique nickel powders with a branched chain or “filamentary” morphology. These powders are produced by the nickel carbonyl decomposition process, described elsewhere [4]. The filamentary powders are characterized by two measurements: the Fisher Sub-Sieve Analyzer (FSSA) (ASTM B330) and the Scott Volumeter (ASTM B229). The FSSA measures average particle size by pressure drop across a uniformly packed bed of the powder under a controlled flow of air, the particle size measured by this method is roughly related to the average filament thickness. The Scott measurement measures the apparent density of the powder, it is roughly related to the chain length. Both of these methods are easy to perform and are standards in the industry for characterizing filamentary nickel powder [5–7].

Since the 1950s, Inco Limited, and now CVRD Inco Limited, has supplied Type 255^{TM} powder for the sintered electrode application. Recently, a new low-density variant of Type 255^{TM}, sold as Type 240^{TM} has been commercialized. A number of samples of nickel powder with low density were made at CVRD Inco’s Clydach Nickel Refinery in an industrial reactor of the type described elsewhere [8]. The Fisher particle size and the apparent density were varied independently in the dataset. In addition to the Fisher particle size and the apparent density, the volume size distribution was measured by laser light scattering using a Malvern Mastersizer 2000. For the measurement of laser light scattering, the samples were dispersed in a dilute water mixture with a surfactant and continuous ultrasonic agitation. Under these conditions, it is expected that the size distribution should be a measure of the average three-dimensional projection of each filamentary particle. The relationship between apparent density and the mode of the volume distribution obtained with the Malvern Mastersizer 2000 is shown in Fig. 2. This figure shows that the average particle diameter calculated from laser light scattering (which is considered to depend on average chain length of the particles) is not perfectly correlated with the apparent density. This is because other factors such as chain branching of the particles (number, length and type of branches) as well as surface smoothness can have an impact on particle packing. Nevertheless, Fig. 2 shows that the apparent density is a reasonable surrogate for indirectly measuring the average chain length of filamentary powders. In this figure, the density specification range for Type 255^{TM} and Type 240^{TM} are also shown, which identifies the key difference between these two commercial grades. In Section 4, we will propose some explanations for the impact of average particle chain size on the characteristics of nickel plaques.

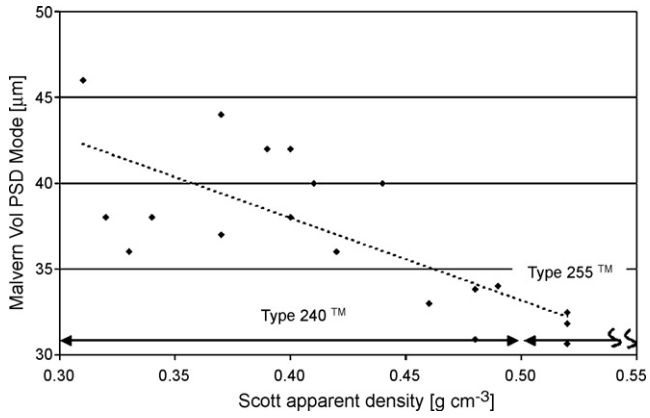

Fig. 2. The relationship between apparent density measured by Scott Volumeter and average particle length measured by laser light scattering (Malvern Mastersizer 2000).

To evaluate and compare the benefits of Type 240^{TM} in the sinter/slurry application, each step of the sinter/slurry process is simulated in this study. Four nickel powders are initially studied, Type 255^{TM}, manufactured Lots B089K and B279X and Type 240^{TM}, manufactured Lots S15 and B547W. The powder properties of each Lot are shown in Table 1.

An aqueous solution of methyl cellulose was made using 3 wt.% A4M methyl cellulose by Dow Chemical following the manufacturer's recommendations. In general, slurries of Type 240^{TM} have a higher viscosity than slurries of Type 255^{TM} at the same solids loading. For this reason, the solids loading of Type 255^{TM} is 54 g nickel powder/100 g of solution, while the Type 240^{TM} solids loading is initially set at 30 g nickel powder/100 g of solution. The slurries are hand-mixed under low shear, to prevent damage of the filaments.

A perforated nickel coated metal strip is manually coated with an excess of nickel slurry and is pulled through a lab-scale vertical tape caster similar to the apparatus described in Ref. [3]. The green plaques are approximately 5 cm × 15 cm in size. These are dried in a lab oven in dry air at about 150 °C for 10 min. The green thickness of the plaques is approximately 0.7 mm. For each condition studied, three plaques are made to verify the level of reproducibility of this lab method.

To simulate the binder burnout and sintering stage, the dried plaques are fired in a single-stage tube furnace. The atmosphere was selected to have oxygen potential that is sufficient to remove the carbonaceous binder material, yet sufficiently reducing to avoid oxidation of the nickel. A mixture of 2% hydrogen, 2% water in a balance of nitrogen is sufficient to obtain this objective. To demonstrate the effect of process conditions on plaque properties the temperature and time of firing is varied between 850 °C and 1 min and 1150 °C and 30 min.

Table 1
Powder properties of Type 255^{TM} and Type 240^{TM} used in this study

Sample	Powder metrics	
	AD (g cm^{-3})	Fisher (µm)
Type 255^{TM}/B089K	0.61	2.35
Type 255^{TM}/B279X	0.53	2.45
Type 240^{TM}/S15	0.33	2.15
Type 240^{TM}/B547W	0.37	2.15

After firing, the porosity and adhesion strength of each group of sintered plaques is measured. The porosity, or voids fraction of each plaque, is measured by cutting out 33.5 mm × 15 mm samples and measuring the volume and weight of the cut-out, subtracting the contribution of the metal strip in each sample. The reported porosity measurement is taken as the average of two individual measurements. For the adhesion strength test, a 6 mm × 6 mm square aluminum stub with a stem is bonded parallel to the top face of a 12 mm × 12 mm cut-out of the plaque, which is mounted to a ceramic backing. All of the bonding is done with an epoxy-based adhesive. The stem is attached to a tensile testing machine, in this case a Sebastian Mark 5 tester (Quad Group, Spokane, Washington, USA) and the normal force is recorded for the yield point where the stub is removed. This is divided by the area of the sample stub to give the plaque strength. This technique is used to measure the adhesion strength at six positions on the plaque and the reported adhesion strength is the average of all six measurements.

The average plaque porosity and adhesion strength for plaques made using Type 255^{TM} Lot B089K and Type 240^{TM} Lots S15 and B547W at different sintering conditions are included in Table 2 and plotted in Fig. 3. Note the inverse relationship between plaque strength and plaque porosity, which is the normative relationship between these two variables. This is sometimes referred to as the "standard operating curve" of the nickel powder. This data shows that the selection of manufacturing conditions for commercial plaques is an optimization exercise, to get the maximum porosity (which represents less nickel powder use) while achieving the minimum required strength as determined by the application requirements.

There are a few more interesting features of Fig. 3. In general, more aggressive sintering conditions such as higher temperature and longer firing time result in lower porosity and higher strength. This is expected since the nickel–nickel diffusion constant is a thermally activated parameter [9]. Increased sintering will increase the adhesion of the nickel powder with itself and the substrate, but will also tend to result in a collapsed, low porosity structure. Secondly, the strength/porosity behaviour of Type 255^{TM} and Type 240^{TM} do not fall onto the same line. Each powder is sufficiently differentiated to have unique performance for making sintered plaques. Thirdly, the Type 240^{TM} operating curve (hatched line) lies to the right hand side of the Type 255^{TM} curve (solid line), suggesting at least hypothetically that the sinter/slurry process could be adapted to make plaques from Type 240^{TM} that would have higher porosity at the same level of strength as plaques made from Type 255^{TM}.

To determine the combined level of reproducibility of the laboratory plaque-making and measurement techniques used in this study, the process of making and measuring the properties of plaques is repeated with B089K (Type 255^{TM}) and B547W (Type 240^{TM}). Three additional sets of slurries and plaques were made using B547W and four additional sets of slurries and plaques are made using B089K, all under the sintering conditions of 1050 °C and 1 min. The results are shown in Table 3. These

Table 2
Plaque porosity and strength as a function of temperature/time for B089K, S15 and B547W

Sample ID	Sintering conditions	Plaque thickness (mm)		Average porosity (%)	Average adhesion strength (kPa)
		Green	Fired		
T.255 B089K	850 °C/1 min	0.70	0.65	88.2	586
T.255 B089K	850 °C/10 min	0.70	0.58	87.1	1375
T.255 B089K	1050 °C/1 min	0.70	0.58	86.9	1150
T.255 B089K	1050 °C/1 min	0.67	0.55	87.4	807
T.255 B089K	850 °C/1 min	0.72	0.66	88.8	363
T.255 B089K	850 °C/10 min	0.72	0.59	87.0	808
T.255 B089K	1050 °C/1 min	0.72	0.61	87.7	762
T.255 B089K	1050 °C/10 min	0.74	0.50	84.9	1787
T.255 B089K	850 °C/1 min	0.71	0.65	88.5	370
T.255 B089K	850 °C/10 min	0.73	0.59	87.3	1212
T.255 B089K	1050 °C/1 min	0.71	0.58	87.1	1212
T.255 B089K	1050 °C/10 min	0.72	0.49	83.9	2284
T.255 B089K	850 °C/1 min	0.71	0.65	88.9	351
T.255 B089K	850 °C/10 min	0.71	0.57	87.1	1348
T.255 B089K	1050 °C/1 min	0.72	0.61	87.7	687
T.255 B089K	1050 °C/10 min	0.72	0.49	84.2	1878
T.240 S15	850 °C/1 min	0.63	0.58	92.4	175
T.240 S15	850 °C/10 min	0.64	0.54	91.9	261
T.240 S15	1050 °C/1 min	0.65	0.54	92.0	267
T.240 S15	1050 °C/10 min	0.65	0.46	90.3	549
T.240 B547W	850 °C/1 min	0.58	0.55	91.7	95
T.240 B547W	850 °C/10 min	0.58	0.54	91.5	265
T.240 B547W	1050 °C/1 min	0.58	0.52	91.0	236
T.240 B547W	1050 °C/10 min	0.59	0.46	90.3	501
T.240 B547W	1050 °C/30 min	0.55	0.39	88.3	970
T.240 B547W	1150 °C/10 min	0.57	0.40	87.7	1000
T.240 B547W	1150 °C/30 min	0.58	0.35	87.2	1550
T.240 B547W	1150 °C/60 min	0.57	0.33	86.3	2106

results can be used to estimate a 95% confidence interval for plaque porosity and adhesion strength. These confidence intervals (shown in Fig. 3) capture the variation inherent in plaque casting, sintering and measurement.

It should be noted that nickel plaques with higher porosity, containing less nickel in cross-section, would also have higher electrical resistivity. A standard four-point electrical resistance probe is used to measure the relationship between electrical resistivity versus volume nickel content (volume nickel content = 100% − porosity). The results are shown in Fig. 4.

During the fabrication of these plaques it was observed that the thickness of the plaques made from Type 240™ was a little

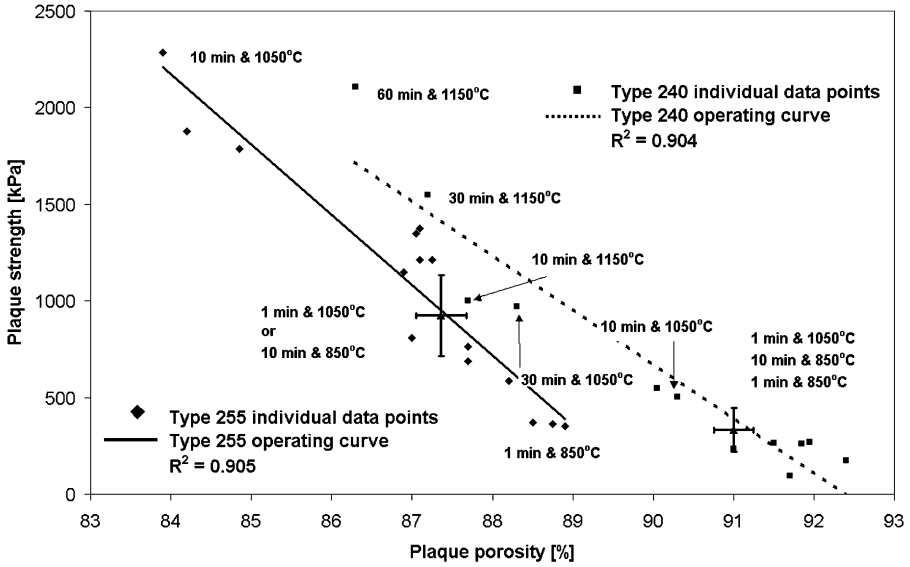

Fig. 3. The relationship between adhesion strength and porosity for nickel plaques made with Type 255™, Lot B089K and Type 240™, Lots S15 and B547W, and fired under different conditions.

Table 3
Plaque porosity and strength of B089K, B547W and B912X replicates at 1050 °C and 1 min

Sample ID	Plaque thickness (mm)		Average porosity (%)	Average adhesion strength (kPa)
	Green	Fired		
B547W	0.58	0.52	91.0	236
B547W first repeat	0.54	0.46	90.7	279
B547W second repeat	0.56	0.47	91.1	504
B547W third repeat	0.55	0.46	91.3	319
B547W 95% confidence interval			[90.8, 91.3]	[222, 448]
B089K	0.67	0.55	87.4	807
B089K first repeat	0.70	0.58	86.9	1150
B089K second repeat	0.72	0.61	87.7	762
B089K third repeat	0.71	0.58	87.1	1212
B089K fourth repeat	0.72	0.61	87.7	687
B089K 95% confidence interval			[87.0, 87.7]	[713, 1134]
B912X	0.67	0.58	90.2	577
B912X first repeat	0.66	0.54	90.4	363
B912X second repeat	0.65	0.55	90.4	426
B912X third repeat	0.61	0.51	89.8	552
B912X 95% confidence interval			[89.9, 90.5]	[378, 582]

bit less than the plaques made from Type 255™ and this was attributed to a slightly lower slurry viscosity during tape casting. Although the doctor blade gap can be adjusted to compensate for changes in the slurry viscosity, it is ideal to be able to modify the solids loading to maintain a constant viscosity during slurry coating.

To be able to understand how the type of nickel powder affects the slurry rheology, a rheometer is used to measure the apparent viscosity as a function of shear rate. For these measurements, we used a Model SR5 rheometer by Maple Instruments. The apparent viscosity is measured in P (1 P = 0.1 Pa s) and the shear rate is varied from $< 0.1\ s^{-1}$ to approximately $100\ s^{-1}$. A solution of 3 wt.% methyl cellulose was used to make up five powder slurries for Type 255™ Lot 279X and another five powder slurries comprised of Type 240™ Lot 547W. The slurries varied in solids loading from 30 g nickel/100 g of solution to 70 g nickel/100 g of solution. As an example of the behaviour of these slurries, the results for Type 255™ Lot B279X are shown in Fig. 5. By plotting the shear stress against shear rate (not shown here), it was demonstrated that these solutions behave as pseudo-plastic fluids, a power law relation can be used to describe the dependence of viscosity on shear rate [10].

Using this data, the apparent viscosity for slurries made from Type 255™ and Type 240™ can be re-plotted as a function of solid loading for a single shear rate. Each curve shows the relative sensitivity of the apparent viscosity to solids loading at one shear rate of interest. In principle, this analysis could be extended to all shear rates in the range from $<0.1\ s^{-1}$ to $100\ s^{-1}$. Fig. 6A–C shows the relationships for shear rates of $1\ s^{-1}$, $6\ s^{-1}$ and $40\ s^{-1}$. In general, slurries made from Type 240™ will have higher apparent viscosity than slurries made from Type 255™ at the same solids loading. The level of dilution that is required to modify a Type 240™ slurry so that it has the same apparent viscosity as a slurry of Type 255™ can be estimated by drawing a horizontal tie line between the Type 255™ curve to the point of intersection with the Type 240™ curve. Reviewing these curves in descending order, it can be seen that the difference in viscosity of the slurries becomes less as the shear rate is increased. Nevertheless, it is obvious that the

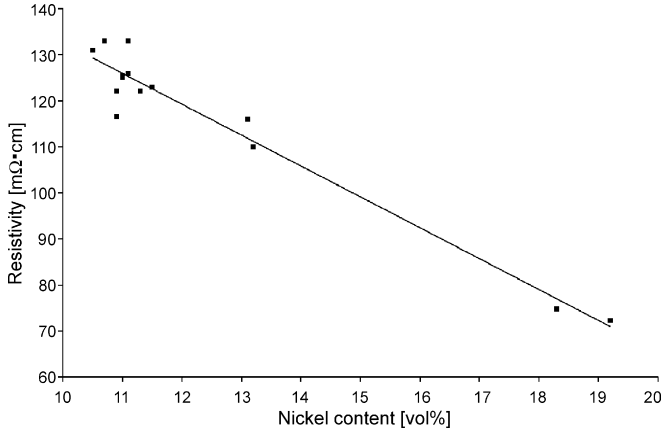

Fig. 4. Sintered plaque resistivity as a function of nickel volume percent (nickel volume percent = 100 − porosity) for a variety of nickel plaques.

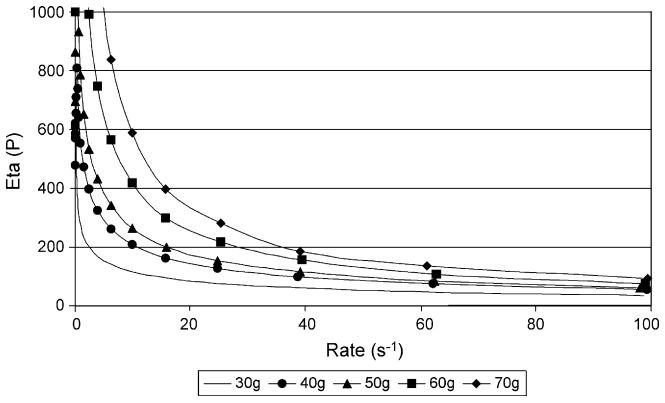

Fig. 5. Apparent viscosity as a function of shear rate for slurries of Type 255™ Lot B279X made at different solids loading.

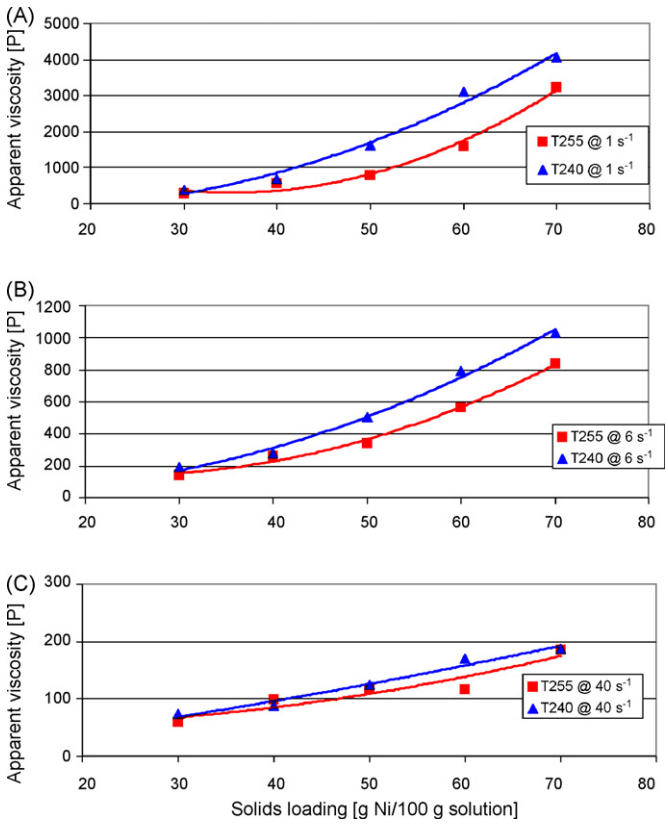

Fig. 6. Apparent viscosity as a function of solids loading for slurries of Type 255™ Lot B279X and Type 240™ Lot B547W: (A) at a shear rate of 1 s^{-1}; (B) at a shear rate of 6 s^{-1}; (C) at a shear rate of 40 s^{-1}.

reduction in solids loading that was employed when we switched from slurries of Type 255™ to Type 240™ (from 54 g/100 g to 30 g/100 g) was too severe, a reduction in solids loading from 54 g/100 g to about 40–45 g/100 g should be adequate to preserve the apparent viscosity of the slurry across the range of shear rates that is appropriate for sintered nickel plaque making. In Section 4, we will show an example calculation for estimating the characteristic shear rate of the sinter/slurry process.

With a better understanding of how to make slurries from Type 240™ without changing the rheological characteristics of the slurry, a wide range of Type 240™ powder Lots are made at Inco CVRD's Clydach Nickel Refinery. The purpose is to determine if there are preferred ranges of powder properties for making sinter plaques. A map of the Scott apparent density versus Fisher particle size is shown in Fig. 7 and the properties are recorded in Table 4. The procedure already described for making slurries is repeated for each powder except that all slurries are made with a constant solids loading ratio of 40 g nickel powder/100 g solution. The slurry viscosity at a shear rate of 1 s^{-1} are also measured for each slurry. Each slurry is pasted and tape-cast using the method described and all plaques are sintered for 1 min at 1050 °C. Plaque porosity and adhesion strength are measured by the technique already described. To assess the reproducibility of the experimental method and measurement techniques, three additional replicates are run of B912X, shown in Table 3.

3. Calculations and results

At the beginning of this study, it is important to determine if the difference in powder morphology and structure between Type 255™ and Type 240™ can be identified as the basis for a statistically significant improvement in plaque characteristics. As shown in Table 2 and Fig. 3, it is well known that sintering conditions can be modified to adjust the porosity and adhesion strength of the plaque, moving it along the standard sinter/slurry operating curve. To determine whether the two operating curves shown in Fig. 3 are distinct, the data in Table 2 is used to calculate the confidence intervals for each sinter/slurry operating curve. This can be calculated using the equation for the variance of a linear form, where the straight line is a reasonable representation of the modeled relationship [11]. The operating curves shown in Fig. 3 are re-plotted with the 95% confidence band around each regressed line in Fig. 8. The confidence bands around each of these lines indicate the region where there is 95% certainty that the true linear relationship exists. In Fig. 8,

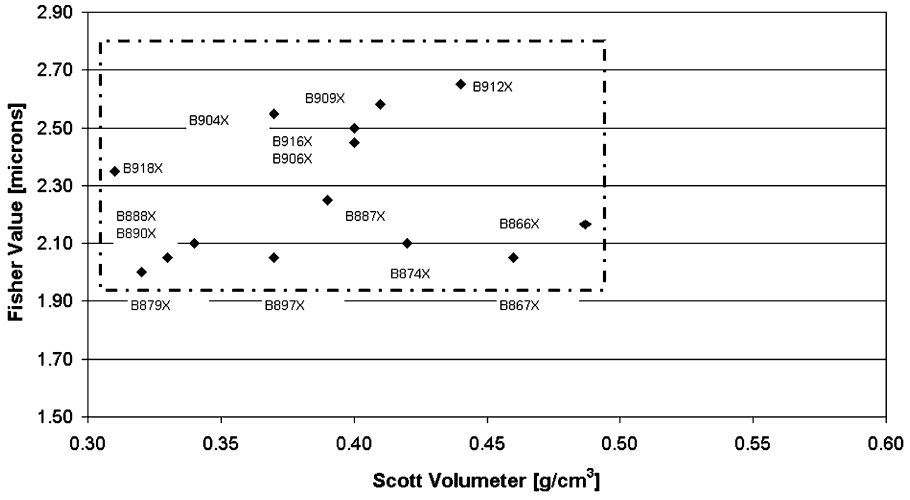

Fig. 7. Variation of Fisher value (primary particle size) and Scott apparent density (inversely proportional to chain length) for the powders investigated in this study.

Table 4
Powder and plaque properties for Type 240™ Lots all sintered at 1050 °C for 1 min

Sample ID	Powder properties				Plaque properties			
	FV (μm)	AD (g cm^{-3})	PSD volume mode (μm)	Slurry apparent viscosity (P)	Thickness (mm)		Average porosity (%)	Average adhesion strength (kPa)
					Green	Fired		
B866X	2.20	0.49	34	159	0.61	0.54	89.8	1129
B867X	2.05	0.46	33	229	0.63	0.54	90.2	504
B874X	2.10	0.42	36	308	0.64	0.52	89.3	986
B879X	2.00	0.32	38	891	0.77	0.67	91.1	574
B887X	2.25	0.39	42	260	0.63	0.53	89.4	591
B888X	2.10	0.34	38	618	0.77	0.61	91.0	837
B890X	2.05	0.33	36	589	0.78	0.65	90.8	535
B897X	2.05	0.37	37	556	0.76	0.62	90.8	900
B904X	2.55	0.37	44	334	0.70	0.55	90.1	720
B906X	2.45	0.40	38	313	0.62	0.58	90.2	389
B909X	2.58	0.41	40	257	0.64	0.54	90.0	604
B912X	2.65	0.44	40	313	0.67	0.58	90.2	577
B916X	2.50	0.40	42	283	0.67	0.57	90.4	431
B918X	2.35	0.31	46	835	0.82	0.71	92.1	319

the confidence regions for both curves are non-overlapping for porosities greater than about 87%. This verifies the original hypothesis, that the lower density Type 240™ powder produces plaques that have an improved combination of performance characteristics compared with plaques made from Type 255™. The next step is to determine which kinds of Type 240™ offer the improved sinter/slurry benefit.

Using the same approach as above, the porosity/strength operating curve and its associated 95% confidence bands are calculated for the variants of Type 240™ shown in Table 4 and Fig. 7. This is shown in Fig. 9. Fig. 9 also has the associated 95% confidence region calculated from replicates plaques made with B912X from Table 3 as an estimate of the error associated with making and measuring plaque properties for each of the powder Lots. Although there is some scatter in the individual results, the plaques as a group form the typical inverse relationship between plaque strength and porosity. In fact, this data fits nicely into the population of Type 240™ plaque properties derived from B547W and S15 in Figs. 3 and 8. In Fig. 9 however, all of the plaques are sintered under identical conditions, so that it is differences in individual powder properties that determine where each plaque will project onto the standard operating line. For example, according to this dataset, B918X produces plaques with the highest porosity and lowest strength while B887X and B874X will tend to produce plaques with the highest strength and lowest porosity.

From the point of view of using Type 240™ in the industrial sinter/slurry process shown in Fig. 1, it is important to have minimum variability in the important properties of each Lot of nickel powder that is used. This is because the manufacturing processes discussed in Section 1 are fine tuned around the major raw materials, and any deviation in properties will have an effect on product performance and reproducibility. Thus, it becomes important to have some powder measurement that can be used to predict where the powder will end up on the standard operating curve, as shown in Fig. 9, when it is cast into a plaque and fired

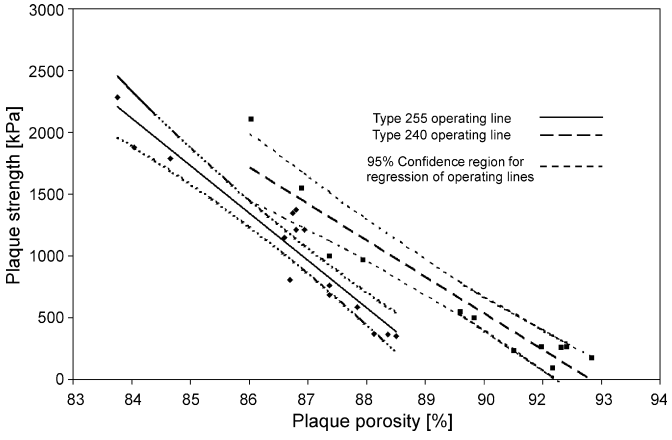

Fig. 8. Strength/porosity curves from Fig. 3 plotted with their 95% confidence bands. These bands are non-overlapping for porosity greater than 87%, suggesting that the two types of powder produce structures with significantly different performance.

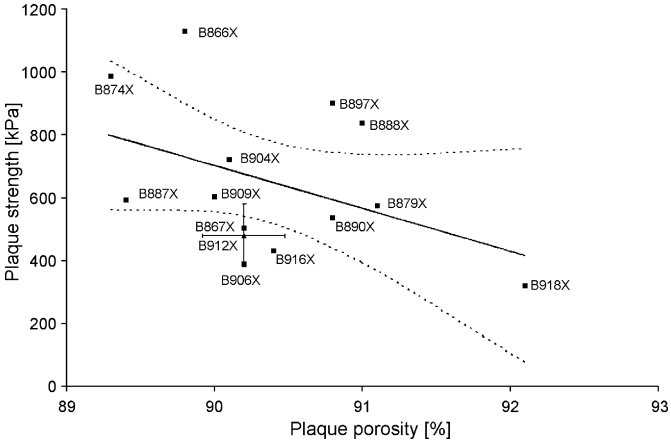

Fig. 9. Strength/porosity curves for the 14 variants of Type 240™ from Table 4, all tape-cast, dried and fired under identical conditions. The cross-bars show the confidence intervals determined experimentally for B912X using three replicates (shown in Table 3).

Table 5
Matrix of correlation coefficients for data in Table 4

	Fisher	Apparent density	Viscosity at 1 s^{-1}	Malvern mode	Green thickness	Sinter thickness	Porosity	Adhesion Strength
Fisher	1.00							
Apparent density	0.22	1.00						
Viscosity at 1 s^{-1}	−0.40	−0.88	1.00					
Malvern mode	0.61	−0.48	0.25	1.00				
Green thickness	−0.32	−0.87	0.92	0.31	1.00			
Sinter thickness	−0.25	−0.80	0.93	0.27	0.90	1.00		
Porosity	−0.16	−0.72	0.85	0.32	0.88	0.94	1.00	
Adhesion Strength	−0.35	0.37	−0.25	−0.48	−0.20	−0.40	−0.42	1.00

under standard conditions. To determine the best nickel powder measurement for predicting plaque performance based on this dataset, the powder and plaque properties in Table 4 are used to develop a matrix of correlation coefficients between the individual properties, which is shown in Table 5. The correlation coefficient between two variables is equal to the covariance of the two properties divided by the square root of the product of the individual variances [11]. Values of the correlation coefficient close to +1 indicate a strong positive correlation between the variables, values close to −1 indicate a strong negative correlation, and values near zero indicate a poor correlation. This correlation matrix has some interesting features, which will be discussed next.

In this matrix, the first four variables (Fisher value, apparent density, viscosity at 1 s^{-1} and Malvern mode) are all properties of the powder and can in general be measured on the powder to predict performance. The next four variables (green thickness, sintered thickness, porosity and adhesion strength) are properties of the plaque. It should be pointed out that the laboratory set-up used in these experiments does not perfectly correspond to the industrial sinter/slurry process, so we are careful not to say that these relationships will hold true generally. With that statement in mind, the data from these experiments suggest the best single powder property that can be used to predict plaque porosity is the slurry apparent viscosity at a constant solids loading and 1 s^{-1} shear rate followed by the Scott apparent density (inversely correlated). The best single predictor of the adhesion strength is the Malvern Mastersizer 2000 mode (inversely correlated), followed by the Scott Volumeter apparent density. Interestingly, there is a very high degree of correlation between the plaque thickness and the viscosity. This analysis suggests that the slurry viscosity has a strong positive effect on the plaque thickness as well as the plaque porosity.

4. Discussion

The results above indicate that nickel powder with a lower apparent density (or longer chain length) can be used to manufacture sintered nickel plaques with characteristic strength/porosity behaviour that is significantly improved over the existing product (Type 255^{TM}) that is dominant in the industry. In particular, sintered plaques can be made with less nickel and the same strength. This can be seen by referring to Fig. 8. If a horizontal tie line is drawn on this graph at 500 kPa, it will intersect the Type 255^{TM} curve at about 88.7% porosity and the Type 240^{TM} curve at 90.7%. In other words, the lower density powders will allow plaques to be made that contain 18% less nickel and the same strength. In addition, there are other benefits of lower porosity such as greater flow permeability through the plaque and improved flexibility during coiling.

The drawbacks of using a lower density powder are twofold. The resistivity of the plaque is increased, as shown in Fig. 4. These results show that the increase in resistivity is directly proportional to the removal of nickel from the plaque cross-section. Secondly, to facilitate the conversion from Type 255^{TM} to Type 240^{TM}, the slurry viscosity should be adjusted so that the plaque after tape casting will retain the same thickness. Alternatively, the gap between the doctor blades could be adjusted so that the final thickness is unchanged. The second alternative is not as satisfactory since it would require a number of feedback iterations before reaching the desired thickness. As well, there may be other parts of the sinter/slurry process that would change if the slurry viscosity was drastically upset.

Although there are a number of dynamic processes in the sinter/slurry process (Fig. 1) that are affected by the slurry viscosity, probably the most important of these is the tape-casting process. During the tape-casting process, it is the viscosity of the paste as it is pulled up between the doctor blades that has a major impact on the thickness of plaque, as suggested experimentally by the high degree of correlation between viscosity and plaque thickness shown in Table 5. To estimate the typical range of shear rates that are characteristic of the tape-casting process, a simplified schematic is shown in Fig. 10. As the slurry-coated metal strip

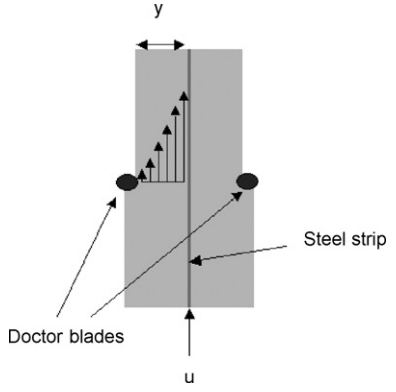

Fig. 10. A simplified schematic of the tape-casting process in cross-section. The light gray is nickel slurry attached to the central metal strip. The metal strip is traveling at a speed u, and the transverse distance between the strip and the edge of the doctor blade is y.

is pulled between the doctor blades, there is a velocity gradient across the thickness. The velocity of the strip is represented as u (m s^{-1}) and the thickness between the strip and the surface of the slurry is represented as y (m). If the "no-slip" condition exists at the interface between the strip and the slurry, and the velocity at the tip of the doctor-blade is approximately zero, then the shear rate du/dy can be approximated as u/y. For a typical range of $u = 0.8$–1.2 m s^{-1} and $y = 0.4$–0.6 mm, the range of shear rates that characterize this step of the process is ∼20–50 s^{-1}. Referring to Fig. 6C which is the apparent viscosity corresponding to a shear rate of 40 s^{-1}, a horizontal tie line drawn from the Type 255^{TM} curve at a typical solids loading of 50 g indicates that a reduction in solids loading of about 15% is sufficient to maintain constant viscosity when replacing Type 255^{TM} with Type 240^{TM}. Of course, this is just an example calculation, and more detailed information would have to be used for replacing Type 255^{TM} with Type 240^{TM} in a specific sinter/slurry process.

The strong inverse correlation between the apparent density and the slurry viscosity can be explained by considering that the apparent density is a direct measure of the space that is occupied by individual particles when there is minimal consolidation. Provided that the particles are not fragmented or mutually attracted during the slurry-making process, low-density powder should behave similarly in the slurry, in other words, it should occupy more volume for the same solids loading. If this is the case, simplified expressions such as Einstein's equation (Eq. (2)) should be applicable for defining the effect of apparent density on slurry viscosity [12]:

$$\mu = \mu_0(1 + \tfrac{5}{2}\phi) \quad (2)$$

ϕ is the volume fraction of the solid, μ_0 the viscosity without solids and μ is the slurry viscosity. If the propensity of the powder to occupy more volume, as measured by the apparent density in air, is also true for powder in a slurry, then ϕ in Eq. (2) should be inversely proportional to the apparent density, and according to Eq. (2), also inversely proportional to the viscosity. It should be pointed out that there are some differences between the nickel powder slurries studied here and the assumptions in Einstein's analysis; Einstein assumed that the particles were spherical and the slurries were very dilute. Nevertheless, the inverse correlation between apparent density and slurry viscosity is in qualitative agreement with Einstein's first principles-based result. In fact, the magnitude of the correlation coefficient between slurry viscosity and porosity is even greater than the magnitude of the correlation coefficient between apparent density and porosity (the correlation coefficients are 0.85 versus −0.72, respectively, as shown in Table 5). This suggests that slurry viscosity is a better predictor of plaque porosity than apparent density. This is probably because the apparent density measurement is susceptible to powder consolidation or mishandling, while the slurry viscosity is more absolute, provided that the particle chains are not damaged. The relationship between porosity and slurry apparent viscosity at 1 s^{-1} is shown in Fig. 11. The correlation coefficient for these two variables is shown in Table 5. The well-known R^2 statistic for quantifying

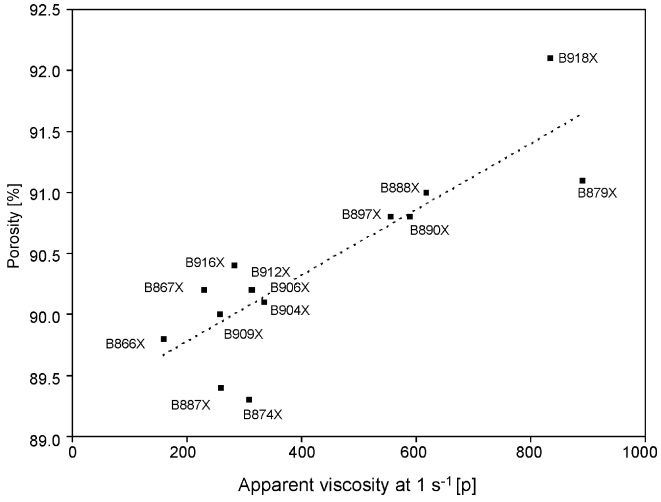

Fig. 11. Plaque porosity as a function of the slurry apparent viscosity at 1 s^{-1} for the Type 240^{TM} powders tested.

degree of fit for a linear regression is equal to the square of the correlation coefficient.

If the particles can retain their low-density characteristics in the slurry and during the coating process, then it is logical that this feature would be preserved in the final plaque porosity when all other conditions such as sintering remain unchanged. This explains how lower density powders can make plaques with higher porosity and also it provides a basis for understanding how the slurry viscosity is a good measurement for quantifying this effect.

5. Validation with an industrial sinter/slurry process

To verify that the sinter/slurry benefits of Type 240^{TM} reported here can also be expected in an industrial sinter/slurry manufacturing process, industrial-scale trials were performed with standard Type 255^{TM} and three Lots selected from Table 4; B879X, B912X and B916X. These plaques were made on a continuous sinter/slurry casting line, similar to the schematic as shown in Fig. 1, in industrial quantities. Plaques for the nickel cadmium positive and negative electrodes were both made.

The porosity and adhesion strength of plaques from this trial were measured using the methods and apparatus described in Section 2. So that the absolute values of these properties are not disclosed, they have been scaled by the value of the same property of the plaques made with Type 255^{TM}. The scaled data is shown in Table 6. Although there is some measured decrease in the adhesion strength of the positive electrode of plaque made from Type 240^{TM}, this is considered within the acceptable summation of errors introduced in the measurement of the Type 255^{TM} plaques and the Type 240^{TM} plaques. This data confirms the original hypothesis, that the sinter/slurry process can be improved by starting with a new low-density powder.

To evaluate the pore size distribution of these plaques, polished cross-sections were made of each representative plaque. Five images were scanned using a scanning electron microscope (SEM, JEOL 6400) at 100× magnification. These images were imported into the image analysis software package Image Pro

Table 6
Scaled value of plaque porosity and strength for industrially made battery plaques measured by techniques described in Section 2

Powder used to make plaque	Scaled porosity (Type 255™ = 100%) (%)		Scaled adhesion strength (Type 255™ = 100%) (%)		Average pore size (μm)
	Positive	Negative	Positive	Negative	
Type 255™	100	100	100	100	12.7
Type 240™ B879X	102.7	102.5	77	111	12.9
Type 240™ B912X	102.2	102.3	77	101	13.0
Type 240™ B916X	102.5	102.4	80	101	14.0

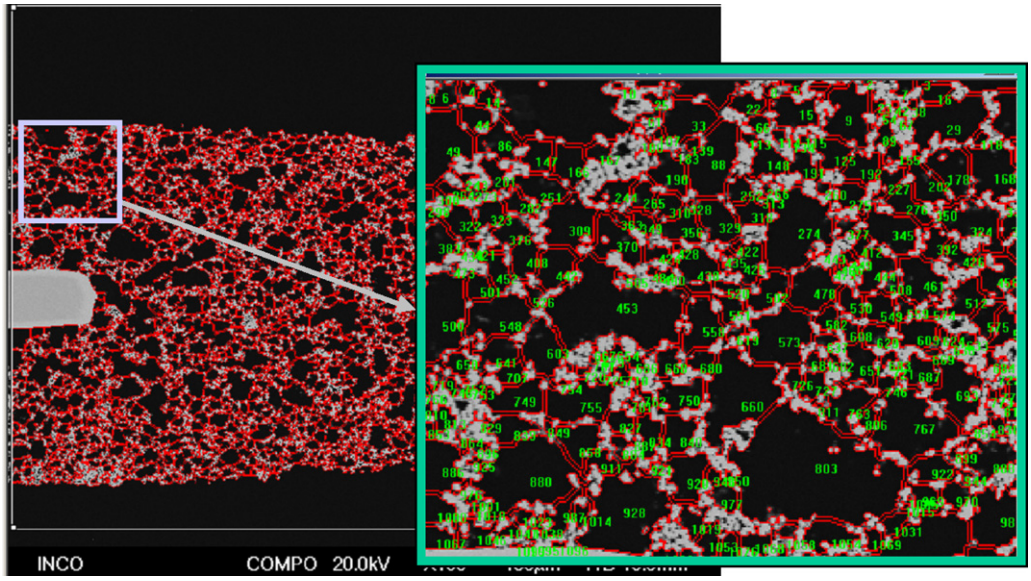

Fig. 12. A plaque cross-section is scanned using an SEM and digitized (background). The image is read into image analysis software and a limited watershed algorithm is used to demarcate individual pores which are measured and counted to estimate the average pore size.

Plus Ver 4.5 (Media Cybernetics, Silver Spring, MD, USA). In this package, a limited watershed algorithm was used to measure the two-dimensional mean diameter and area of each pore in the plaque. Approximately 11,000–12,000 pores were counted per sample and used to compute a number average pore size, which is also included in Table 6. An illustration of how the software was able to identify and measure individual pores is shown in Fig. 12. These results indicate that there is only a modest increase in pore size associated with the reduction of nickel in the plaque. The size of the pores is still an order of magnitude less than nickel foam, typically 200–500 μm.

6. Conclusions

A new basis for making improved nickel plaques by the sinter/slurry process has been explored by introducing a new low density powder which allows new combinations of porosity and strength to be achieved. Under normal sinter/slurry conditions this allows plaques to be made with more open porosity and about 20% less nickel at the same strength. The microstructural feature of the powder that allows this is increased particulate volume. This can be reasonably measured using standard powder metal metrics such as the apparent density, but there is a closer apparent correlation between the slurry viscosity and the plaque porosity, indicating that the slurry viscosity may be a more sensitive predictor of this structural property than apparent density. In general, plaque thickness is very dependent on slurry viscosity, which is higher for low-density powders. A method for evaluating the characteristic shear rate of the process was proposed so that the solids loading of the slurry can be adjusted to maintain constant viscosity. Under typical conditions, a reduction in solids loading of 10–20% is sufficient when using Type 240™ powders in the place of Type 255™.

Acknowledgements

The authors would like to thank the staff at the Clydach Nickel Refinery, Clydach Wales and especially Steve Wilson, Fiona Buttrey, Charlie Eves and Helen Davies, for conducting a trial that allowed us to consider the full range of chain-like nickel powders in this study. Phil Hutchison's contribution in the experimental work is also appreciated. Yukitsugu Ishikawa and Takamitsu Suzuki of the Furukawa Battery Company Limited provided helpful information about sintered electrode properties and technology. We would also like to thank CVRD Inco Limited for permission to publish this study.

References

[1] D. Linden, T.B. Reddy (Eds.), Handbook of Batteries, 3rd ed., McGraw Hill, New York, 2003.
[2] A. Zaitsev, D.S. Wilkinson, G.C. Weatherly, T.F. Stephenson, The preparation of highly porous structures from filamentary nickel powders, J. Power Sources 123 (2003) 253–260.
[3] V.I. Chani, Q. Yang, D.S. Wilkinson, G.C. Weatherly, J. Power Sources 142 (2005) 370–381.
[4] E.B. Wasmund, K.S. Coley, In-situ sampling uncovers the dynamics of particle genesis and growth in an aerosol tube reactor, J. Mater. Sci. 41 (2006) 7103–7110.
[5] B. Kaye, Particle size characterization, in: Handbook of Powder Science and Technology, 2nd ed., Chapman and Hall, New York, 1997.
[6] T. Allen, Particle Size Measurement, Chapman and Hall, New York, 1974.
[7] A. Poster, Handbook of Metal Powders, Reinhold, 1966.
[8] R.A. Bale, E.T. Chapman, Proceedings of the 25th CIM, 1986.
[9] R. German, Sintering Theory and Practice, John Wiley, New York, 1996.
[10] D. Pnueli, C. Gutfinger, Fluid Mechanics, Cambridge University Press, Cambridge, 1997.
[11] G.E.P. Box, W.G. Hunter, J.S. Hunter, Statistics for Experimenters, John Wiley, New York, 1978.
[12] A. Einstein, Ann. Phys. 19 (1909) 289–306.